

Article

Comparative Analysis of Small-Scale Organic Rankine Cycle Systems for Solar Energy Utilisation

Ruiqi Wang, Long Jiang *, Zhiwei Ma, Abigail Gonzalez-Diaz, Yaodong Wang and Anthony Paul Roskilly

Sir Joseph Swan Centre for Energy Research, Newcastle University, Newcastle NE1 7RU, UK; r.wang34@newcastle.ac.uk (R.W.); zhiwei.ma@newcastle.ac.uk (Z.M.); agonzalez-diaz@newcastle.ac.uk (A.G.-D.); yaodongwang@newcastle.ac.uk (Y.W.); aproskilly@newcastle.ac.uk (A.P.R.)

* Correspondence: long.jiang@newcastle.ac.uk

Received: 20 December 2018; Accepted: 26 February 2019; Published: 2 March 2019



Abstract: Small-scale organic Rankine cycle (ORC) systems driven by solar energy are compared in this paper, which aims to explore the potential of power generation for domestic utilisation. A solar thermal collector was used as the heat source for a hot water storage tank. Thermal performance was then evaluated in terms of both the conventional ORC and an ORC using thermal driven pump (TDP). It is established that the solar ORC using TDP has a superior performance to the conventional ORC under most working conditions. Results demonstrate that power output of the ORC using TDP ranges from 72 W to 82 W with the increase of evaporating temperature, which shows an improvement of up to 3.3% at a 100 °C evaporating temperature when compared with the power output of the conventional ORC. Energy and exergy efficiencies of the ORC using TDP increase from 11.3% to 12.6% and from 45.8% to 51.3% when the evaporating temperature increases from 75 °C to 100 °C. The efficiency of the ORC using TDP is improved by up to 3.27%. Additionally, the exergy destruction using TDP can be reduced in the evaporator and condenser. The highest exergy efficiency in the evaporator is 96.9%, an improvement of 62% in comparison with that of the conventional ORC, i.e., 59.9%. Thus, the small-scale solar ORC system using TDP is more promising for household application.

Keywords: organic Rankine cycle; thermal driven pump; small-scale; energy and exergy efficiency

1. Introduction

Solar thermal technology is gathering the momentum to meet household demands for both heating and electricity in the UK [1]. Due to the relatively low annual yield of incident solar radiation, low-temperature heat source recovery technologies have become more significant, e.g., thermoelectric power and the organic Rankine cycle (ORC), when considering thermal efficiency and system compactness [2,3]. Compared with the poor efficiency of thermoelectric power at low solar radiation, the ORC could be a better candidate for distributed household applications, as it is able to operate efficiently and affordably at relatively low working temperatures [4,5].

Considerable progress has been made in the development of solar ORC systems for small-scale power generation [6,7]. With a range of solar collector designs, both concentrating and non-concentrating types had been featured for solar ORC systems [8,9]. An overall efficiency of 4.2% was obtained by using evacuated tube collectors and 3.2% using flat-plate collectors [10]. Other concentrating parabolic through collectors demonstrated higher overall efficiencies in the region of 7.5–12.1% [6,11]. The nanofluid was utilised in a solar driven ORC with parabolic trough collectors to achieve a higher system performance and the system efficiency was found to be 20.11% [12].

An onsite experimental evaluation of a low temperature solar ORC system was presented for reverse osmosis desalination. However, considerably low efficiency was observed [13]. Combined solar heat and power system based on the ORC cycle have advantageous ability to use low-cost thermal energy storage to provide continuous operation under intermittent solar-irradiance conditions [14]. A number of investigations have proposed thermal energy storage solutions using solid-liquid phase change materials for solar ORC system [15,16]. It is noted that there are vast potentials to further improve thermal performance through the organic working fluid exploration and ORC system optimisation [17,18].

Considering organic working fluids, different applications have been investigated by various researchers [19]. The slope of the saturation curve for working fluids in a temperature vs. specific entropy diagram can be positive, negative and vertical, which are correspondingly named “wet”, “dry” and “isentropic” fluids [20]. Wet fluids (e.g., water) are usually required to be superheated, whereas many other organic fluids may be dry or isentropic, which do not need superheating. Another advantage of organic working fluid is that a turbine established for ORCs typically requires only a single-stage expander, which brings about a simpler and more economical system in terms of cost and maintenance [21]. Common pure working fluids, e.g., R123 [22], R245fa [23], R245ca [24] and n-pentane [25], have been comprehensively studied. The mixtures are also developed and attempted for ORCs [26,27]. Thermophysical properties of working fluids, e.g., fluid density and thermal conductivity, are analysed and summarised, and working fluids can then be selected in terms of the above properties, thermal stability, compatibility, environmental impacts, safety and cost [28]. Based on selection criteria, R245fa and R134a are often regarded as suitable working fluids for recovering a low-temperature heat source [29].

System optimisation can be realized by improving the thermal performance of each component. Among the four main components of the conventional ORC, the expander is the most investigated due to the fact that it is related to the work output [30]. The work output acts as a positive numerator when calculating thermal efficiency [31]. A variety of expanders have been assessed to attempt improving thermal performance, e.g., scroll expander [32,33], piston expander [34], rotary expander [35], screw expander [36,37] and radial turbine [38]. In general, the scroll expander is the most suitable expander for a small-scale ORC system [39]. Recently, several research efforts have aimed to accomplish better performance by using a free-piston expander [40]. Moreover, two heat exchangers serve as the evaporator and condenser for conventional ORC systems. Thus, heat transfer enhancement is conducive to overall system evaluation, which is greatly relevant to heat input as the denominator for calculating thermal efficiency [41]. Different evaporation and condensation processes have been investigated in terms of heat exchanger type, tube structure, refrigerant, etc. [42]. Nonetheless, another item in the equation for calculating thermal efficiency may be easily ignored. Pump work acts as a negative numerator, which consumes electricity in a real application. Pump work in various studies is not included when calculating the overall efficiency. One such case is if the scale of the ORC system is large, i.e., pump work only accounts for less than 5% of the electricity output. Thus, pump work will not significantly influence the efficiency, even if it is ignored [43]. The other case is if thermal efficiency has a negative effect on the overall performance. This part is selectively overlooked to present decent results. However, pump consumption becomes even larger for a small-scale ORC when the heat source temperature becomes lower [44].

A possible solution is to realize the ORC without using an electrical driven pump. The pump is generally used to pressurize the refrigerant from condensing pressure to evaporating pressure. The pressure difference is also achievable by other methods. One concept is to use the gravity of the working fluid, i.e., enough height difference between evaporator and condenser [45]. Although the height brings about a pressure difference, the required value becomes a barrier in several applications. An alternative idea is to drive the ORC by using a thermal-driven pump (TDP), which is a thermodynamic way to replace the electrical driven pump [46]. A thermosiphon, i.e., a heat pipe, is one type of thermal driven pump, and it was first proposed in the last century [47]. Due to its

unique characteristic, the power generation is too small. Another thermal driven pump is the pressure difference realized by heating and cooling at intervals [46]. An experimental rig was established to prove the feasibility of this TDP [48]. Our previous work also investigated its working performance by using a lab-scale prototype, but the unstable power output was not satisfactory [49]. Later, a modified experimental rig was built to improve the thermal performance. Results indicated that the efficiency was further improved, and 90% of the power generating process was stable [50]. Due to the characteristic of solar energy, the fluctuation could be accepted by using battery technology. Thus, a solar ORC using TDP may be desirable for domestic application, which is expected to have a higher thermal efficiency when compared with that of the conventional type.

To the authors' best knowledge, few research studies on the solar ORC with TDP are reported. Thus, this paper aims to evaluate the performance of a small-scale ORC with TDP when operating at a low solar irradiance level. To further illustrate its advantages and disadvantages, the performance is compared with that of conventional solar ORC in terms of power output, energy and exergy efficiencies. The overarching framework of this paper is elaborated as follows. Solar ORCs using and not using TDP are presented in Section 2. Then, modelling and evaluation equations are defined in Section 3. Thermal performances of the solar ORCs are compared in Section 4, which is followed by conclusions in Section 5.

2. System Description

Figure 1 indicates the schematic diagrams of combined solar heat and power systems. The solar collector provides the thermal energy for evaporating the working fluid. One water tank between the ORC system and solar collector serves as a heat exchanger, which could be replaced by a thermal energy store vessel where phase change materials can be considered as the storage media. Another water tank could be used to supply the domestic hot water for end users from the heat rejected by the condensation [14]. It will be a reduction in the fuel demand to heat the water. The electricity generation by ORC is set to be prioritised over water heating. A proportion of the solar collector fluid will be transferred to the domestic hot water tank only when the collector fluid is at a higher temperature than the hot water tank plus a pinch difference. When this temperature is higher than the critical temperature of working fluids, excess solar heat is rejected directly to the hot water tank. No heating is delivered to the hot water tank if its mean temperature is above the maximum hot water storage temperature [5]. Since the ORC is the main investigation target, the storage part is not analysed in the rest of this paper.

As shown in Figure 1a, the conventional ORC is mainly composed of two heat exchangers (evaporator and condenser), an expander and a working fluid pump. Its principle is the same as that of the Rankine cycle. Working fluid is pumped into a boiler, where it is evaporated and passes through an expander for power generation. Then, it goes through a condenser, where it is finally condensed. Due to energy consumption of the electrical driven pump, the basic ORC may enjoy a very low energy efficiency when the heating temperature is low and the rated power output is small. To solve this problem, the ORC part replaces the electrical driven pump with TDP, which is shown in the dashed area of Figure 1b.

Figure 2 presents different operation modes of ORC using TDP. The ORC using TDP is mainly composed of two high-efficiency heat exchangers, i.e., heat exchanger 1 and heat exchanger 2, an expander, a generator and other auxiliary components [49]. The working processes consist of a pre-expansion process and a power generation process, which are briefly illustrated as follows: (a) Pre-expansion process. Heat exchanger 1 acts as a condenser while heat exchanger 2 works as an evaporator. Water valves V1, V3, V6 and V8 are open, and all other valves are closed. The evaporator that is full of the working fluid, i.e., heat exchanger 2, undertakes isochoric heating through hot water, and its pressure increases gradually until it becomes constant. Meanwhile, the working fluid in the condenser, i.e., heat exchanger 1, starts as saturated vapour at a high temperature and pressure. The condenser applies an isochoric cooling process. (b) Power generation process. When

the pressure of the evaporator becomes constant and the condenser achieves a cooler level, RV2 and RV4 are opened. Then, the working fluid with high temperature and pressure from the evaporator flows into the expander and generates the power. The power is outputted until there is no pressure difference between the evaporator and condenser. During this process, the high-pressure working fluid in the evaporator is isobarically heated. The exhaust enters the condenser and is condensed into saturated liquid. When the generator does not produce power, RV2, RV4, V1, V3, V6 and V8 are closed. This whole process that is termed as a generalised working cycle is shown in Figure 2a. Then heat exchanger 1 and 2 swap their roles as condenser and expander. A new cycle starts as indicated in Figure 2b, which is similar to previous pre-expansion and power generation processes. A working mode for the ORC using TDP could be according to Table 1. For further clarification of the whole process, different operating modes of water and refrigerant valves for the ORC using TDP are listed in Table 2. It is noted that heat exchangers 1 and 2 are always heated and cooled inversely. No power output is obtained in the pre-expansion process, which slightly reduces the average output.

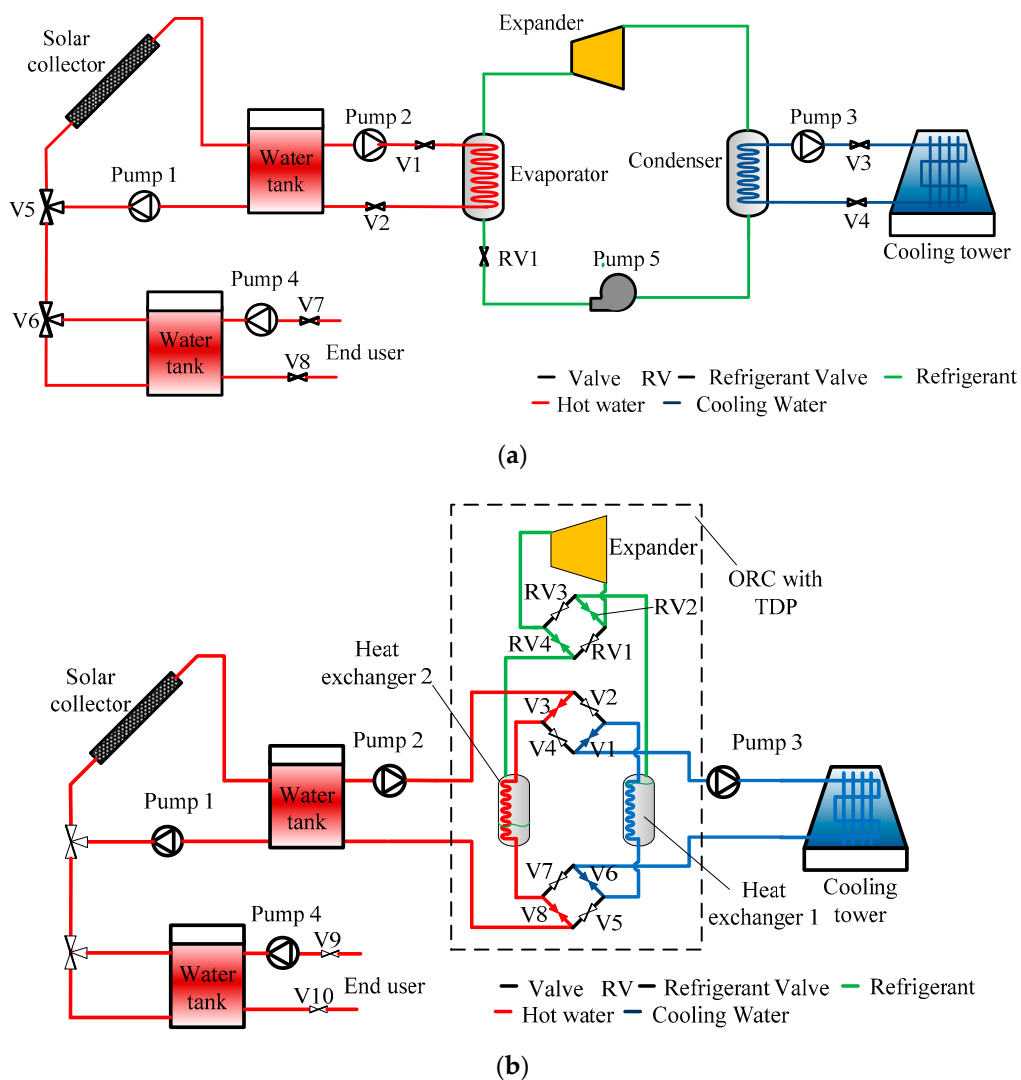


Figure 1. Schematic diagram of combined solar heat and power systems based on (a) the conventional organic Rankine cycle (ORC); and (b) the ORC using thermal driven pump.

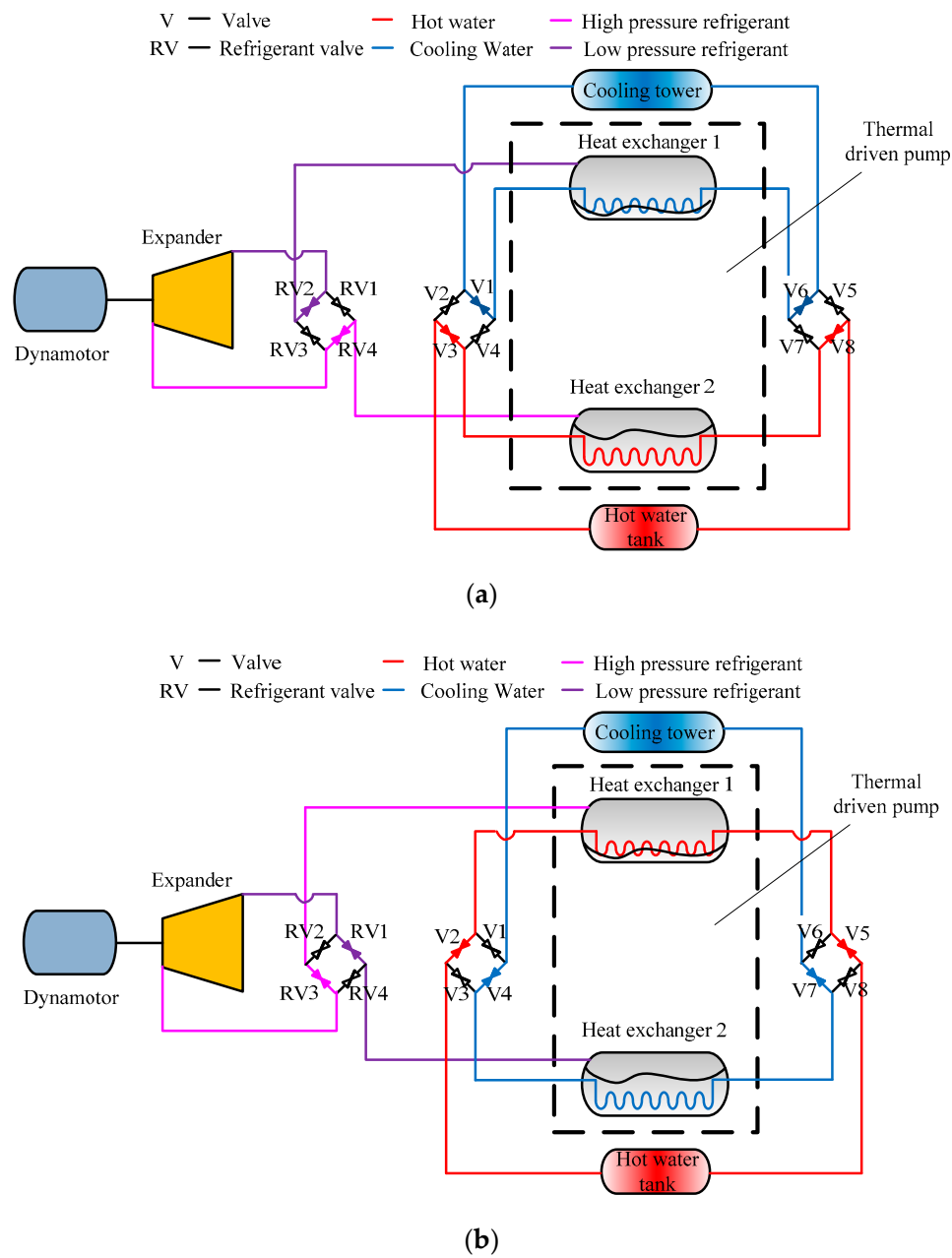


Figure 2. Schematic diagram of ORC with thermal driven pump (a) first cycle; and (b) next cycle.

Table 1. Working mode for the organic Rankine cycle (ORC) using thermal driven pump (TDP).

Working Mode	Pre-Expansion	Power Generation	Pre-Expansion	Power Generation
Heat exchanger 1	Cooling	Cooling	Heating	Heating
Heat exchanger 2	Heating	Heating	Cooling	Cooling
Power	Unable	Able	Unable	Able

Table 2. Different operating modes of valves for the ORC using TDP.

Valves		V1, V3, V6, V8	V2, V4, V5, V7	RV1, RV3	RV2, RV4
First cycle	Pre-expansion	Open	Close	Close	Close
	Power generation	Open	Close	Close	Open
Next cycle	Pre-expansion	Close	Open	Close	Close
	Power generation	Close	Open	Open	Close

In fact, the working fluid pump is replaced by the TDP, i.e., the switch of two heat exchangers as shown in the dashed area of Figure 2. Compared with the conventional ORC, the ORC using TDP may have a higher energy efficiency since the pump is eliminated. Additionally, it is worth noting that continuous power output could be obtained in the power generation process, and thermal continuity is influenced by the pre-expansion process. To solve this problem of continuity, it tends to use two or more ORCs with TDPs for power generation alternatively. However, it is acceptable for the solar ORC, which can utilise battery technology for electricity storage.

A T - s diagram of a solar ORC cycle using a typical working fluid, i.e., R245fa, is shown in Figure 3. The heat is obtained from a solar collector using water as a heat transfer fluid. A fixed superheated temperature difference $\Delta T_{\text{superheated}}$ of $5\text{ }^{\circ}\text{C}$ is assumed between the heat source fluid inlet and working fluid outlet. Thus, the working fluid outlet temperature is evaluated as $T_1 = T_{\text{sc},1} - \Delta T_{\text{superheated}}$. In order to comprehensively evaluate the performance, refrigerants of R245fa, R134a and isobutane are chosen as the working fluids for solar ORC systems. These refrigerants have been verified as well-suited candidates for low-temperature ORC applications due to their thermodynamic and physical properties, low flammability, corrosiveness and environmental impacts [5,20]. The thermodynamic data of these organic compounds are obtained from REFPROP 9 (National Institute of Standards and Technology, Gaithersburg, MD, USA).

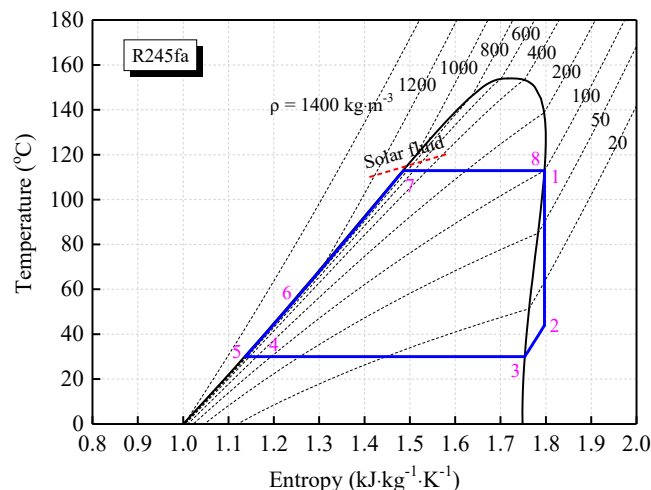


Figure 3. T - s diagram of a solar ORC using R245fa as the working fluid.

3. Methodology

3.1. Aspen Model

The solar ORC model was built in Aspen Plus (v 8.8, Aspen Technology, Inc., Bedford, MA, USA), which includes the specification of each block [51]. The Peng–Robinson method was used to calculate the properties of all the components. Figure 4 shows the schematic diagram of the solar ORC system in Aspen Plus. The relevant assumptions are as follows: (1) The ORC cycle and its components operate under steady-state conditions; (2) thermodynamic equilibrium happens at the inlet and outlet of each component; (3) the kinetic energy of heat transfer and working fluid in solar ORC cycles are negligible; (4) heat loss and pressure drops in the system can be overlooked; and (5) the electricity consumption of water valves and refrigerant valves is ignored. The input parameters in the model are given in Table 3.

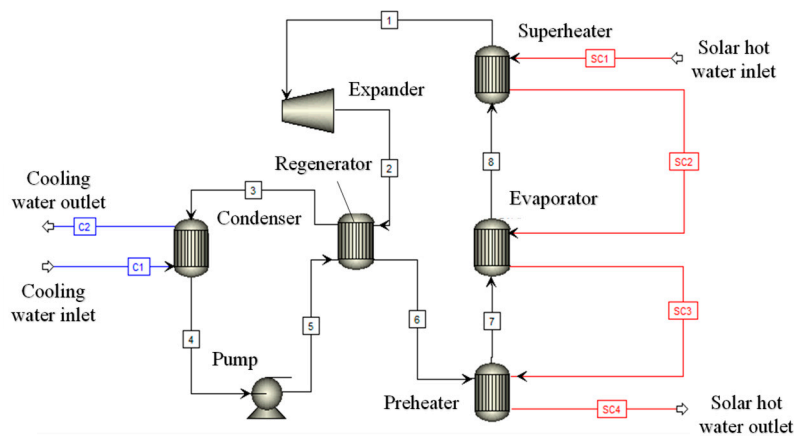


Figure 4. Schematic diagram of the solar ORC model in Aspen Plus.

Table 3. Input parameters of the solar ORC model in Aspen Plus.

Section	Parameter	Value
Fluid pump	Discharge pressure	Evaporating pressure
	Efficiency	0.65
Regenerator	Cold stream outlet temperature	T_6
Preheater	Cold stream outlet vapour fraction	0
Evaporator	Cold stream outlet vapour fraction	1
Superheater	Cold stream outlet temperature	T_1
Expander	Discharge pressure	Condensing pressure
	Isentropic efficiency	
Condenser	Condensation temperature	20 °C
Working fluid	Mass flow rate	0.003 kg·s ⁻¹
	Mass flow rate ^a	0.03 kg·s ⁻¹
Solar collector fluid	Solar hot water inlet temperature ^b	$T_{sc,1}$
	Mass flow rate	0.1 kg·s ⁻¹
Cooling water	Mass flow rate	0.1 kg·s ⁻¹
	Cooling temperature	10 °C

^a Values are taken from the [5]. ^b The solar hot water inlet temperature is adopted from the [52].

3.2. Evaluation of Solar Collector

The proposed solar ORC systems utilise thermal energy absorbed by a solar collector. The useful energy output from the solar collector per m² can be predicted as a function of local climatic conditions using the widely adopted model by Peters and Bales [1,53], which can be expressed as Equation (1):

$$\dot{Q}_{sol} = F'(\tau\alpha)_{en}K_{\theta b}(\theta)I_{sol,b} + F'(\tau\alpha)_{en}K_{\theta d}I_{sol,d} - c_6uI_{sol} - c_1(T_{sc} - T_{ext}) - c_2(T_{sc} - T_{ext})^2 - c_3u(T_{sc} - T_{ext}) + c_4(E_L - \sigma T_{ext}^4) - c_5 \frac{dT_{sc}}{dt} \quad (1)$$

where I_{sol} may be the direct normal or global irradiance depending on the collector type, and c_1 to c_6 are solar collector efficiency curve coefficients. $F'(\tau\alpha)_{en}$ is zero loss efficiency for global or total radiation at normal incidence. K_{θ} is the solar collector incident angle modifier. Furthermore, u is the wind speed in (parallel to) the collector plane and E_L is the long wavelength radiation (outside solar spectrum) onto the collector plane.

For simplicity, the efficiency of the solar collector η_{sc} is calculated as a function of the incident solar irradiance I , the incident angle modifier K_{θ} , the mean collector temperature T_{sc} and the ambient air temperature T_{ext} , which can be expressed as Equation (2) [1,54].

$$\eta_{sc} = \eta_0 K_{\theta} - c_1 \left(\frac{T_{sc} - T_{ext}}{I_{sol}} \right) - c_2 \frac{(T_{sc} - T_{ext})^2}{I_{sol}} \quad (2)$$

where $K_{\theta} = (K_{\theta,b}I_{sol,b} + I_{sol,d}) / (I_{sol,b} + I_{sol,d})$. The possible types of solar collectors that can be used in ORC systems are not reviewed in the present study since the main purpose of this paper is to compare the performance of ORCs using and not using TDP. Thus the type of solar collector is adopted from the reference [1] and the outlet temperature of solar collector array is chosen from reference [52]. The TVP SOLAR HT-Power, a high efficiency evacuated flat-plate collector is selected, and the detailed parameters of the solar collector are listed in Table 4.

Table 4. Solar collector model coefficients [1].

Coefficient	Value
η_0	0.82
c_1	0.399
c_2	0.0067
$K_{\theta,(\theta = 50^\circ)}$	0.91

The energy balance for the collector can be evaluated as Equation (3):

$$M_{sc}c_{p,w} \frac{dT_{sc}}{dt} = \dot{Q}_{sol} + \dot{m}_{sc}c_{p,w}T_{sc,in} - \dot{m}_{sc}c_{p,w}T_{sc,out} \quad (3)$$

where M_{sc} , \dot{m}_{sc} and $c_{p,w}$ are mass, mass flow rate and specific heat capacity of the solar collector fluid, respectively. $T_{sc,in}$ and $T_{sc,out}$ are the inlet and outlet temperature of the solar collector.

3.3. Performance Evaluation of ORC Systems

The performance analysis of solar ORC systems is based on the first and second thermodynamic laws. The general energy balance of the conventional ORC can be expressed as Equations (4) and (5):

$$\sum \dot{m}_{in} = \sum \dot{m}_{out} \quad (4)$$

$$\dot{Q} + \dot{W} = \sum \dot{m}_{out}h_{out} - \sum \dot{m}_{in}h_{in} \quad (5)$$

where \dot{Q} and \dot{W} are the net heat flow rate and work inputs, h is specific enthalpy of the stream of the system, and \dot{m}_{in} and \dot{m}_{out} are inlet and outlet mass flow rates.

The energy balance of working fluids in the solar heating process can be evaluated by Equations (6)–(9):

$$\dot{Q}_{preheat} = \dot{m}_{wf}(h_7 - h_6) = \dot{m}_w(h_{sc,3} - h_{sc,4}) \quad (6)$$

$$\dot{Q}_{eva} = \dot{m}_{wf}(h_8 - h_7) = \dot{m}_w(h_{sc,2} - h_{sc,3}) \quad (7)$$

$$\dot{Q}_{superheat} = \dot{m}_{wf}(h_1 - h_8) = \dot{m}_w(h_{sc,1} - h_{sc,2}) \quad (8)$$

$$\dot{Q}_h = \dot{Q}_{preheat} + \dot{Q}_{eva} + \dot{Q}_{superheat} \quad (9)$$

where $\dot{Q}_{preheat}$, \dot{Q}_{eva} and $\dot{Q}_{superheat}$ are the thermal energy obtained by working fluids in the preheating, evaporation and superheating process, respectively. The subscripts of specific enthalpy h are based on the state points, as shown in Figure 3.

The heat balances in the condenser and regenerator can be expressed by Equations (10) and (11):

$$\dot{Q}_{cond} = \dot{m}_{wf}(h_3 - h_4) = \dot{m}_c(h_{c,2} - h_{c,1}) \quad (10)$$

$$\dot{Q}_{regen} = \dot{m}_{wf}(h_2 - h_3) = \dot{m}_{wf}(h_6 - h_5) \quad (11)$$

Energy conservation in the expander and fluid pump is defined by Equations (12) and (13):

$$\dot{W}_{\text{exp}} = \dot{m}_{\text{wf}}(h_1 - h_2) \quad (12)$$

$$\dot{W}_{\text{pu}} = \dot{m}_{\text{wf}}(h_5 - h_4) \quad (13)$$

Thus, the net power \dot{W}_{net} and cycle thermal efficiency of the conventional ORC η_{ORC} are presented by Equations (14) and (15):

$$\dot{W}_{\text{net}} = \dot{W}_{\text{exp}} - \dot{W}_{\text{pu}} \quad (14)$$

$$\eta_{\text{ORC}} = \frac{\dot{W}_{\text{net}}}{\dot{Q}_{\text{h}}} \quad (15)$$

The exergy analysis of the conventional ORC can be evaluated by Equations (16)–(20):

$$\dot{E} + \dot{W} = \sum \dot{E}_{\text{out}} - \sum \dot{E}_{\text{in}} + \dot{I} \quad (16)$$

$$e = h - h_0 - T_0(s - s_0) \quad (17)$$

$$\dot{E} = \dot{m}e \quad (18)$$

$$\dot{E}_{\text{h}} = \sum \left(1 - \frac{T_0}{T}\right) \dot{Q}_{\text{h}} \quad (19)$$

$$\eta_{\text{ex,ORC}} = \frac{\dot{W}_{\text{net}}}{\dot{E}_{\text{h}}} \quad (20)$$

where \dot{E} and \dot{I} are the exergy rate and irreversibility rate, e is the specific flow exergy, \dot{E}_{h} and η_{exergy} are the heat exergy and exergy efficiency of the conventional ORC, respectively, and T is the temperature of the heat input.

The total heat input of the ORC using TDP is composed of two parts. One is the heat for the evaporation of the refrigerant. The other is the sensible heat for warming up the refrigerant. These are found by Equations (21) and (22):

$$\dot{Q}_{\text{h, TDP}} = \dot{Q}_{\text{wf}} + \frac{1}{t_{\text{cycle}}} \dot{m}_{\text{wf}} c_{\text{wf}} \Delta T_{\text{wf}} \quad (21)$$

$$\dot{Q}_{\text{wf}} = \frac{1}{t_{\text{cycle}}} [\dot{m}_{\text{wf}}(h_6 - h_4) + \int_0^{t_{\text{power}}} \dot{m}_{\text{wf}}(h_1 - h_6) dt] \quad (22)$$

where t_{cycle} is cycle time, which is composed of both pre-expansion and power generation processes.

The average power output can be found by Equation (23):

$$\dot{W}_{\text{ave}} = \frac{1}{t_{\text{cycle}}} \int_0^{\text{cycle}} \dot{W}_{\text{ins}} dt = \frac{1}{t_{\text{cycle}}} \int_0^{\text{cycle}} \dot{m}_{\text{wf}} \eta_s (h_{\text{v}} - h_{\text{exp,out}}) \quad (23)$$

where \dot{W}_{ins} is the instantaneous power output; η_s is the isentropic efficiency; $h_{\text{exp,out}}$ is the outlet enthalpy of the expander.

The energy efficiency of the ORC using TDP can be determined according to Equation (24):

$$\eta_{\text{TDP}} = \frac{\dot{W}_{\text{ave}}}{\dot{Q}_{\text{h,TDP}}} \quad (24)$$

The heat exergy of the ORC with TDP can be calculated by Equation (25):

$$\dot{E}_{h,TDP} = \dot{Q}_{h,TDP} \times \left(1 - \frac{T_0}{T_{h,ave}}\right) \quad (25)$$

where $T_{h,ave}$ is the average temperature of the heat input.

The exergy efficiency of the ORC with TDP can be expressed as Equation (26):

$$\eta_{ex,TDP} = \frac{\dot{W}_{ave}}{\dot{E}_{h,TDP}} \quad (26)$$

3.4. Validation of ORC Model

To validate the ORC model used in this paper, the results in this work are compared with the reference data in Kaşka's work [55] which are shown in Table 5. It is worth noting that the relative errors show a good agreement between the reference and present work. Thus, the ORC model in the present study is reliable to be used in the calculations.

Table 5. Comparison of results between the reference and present work.

Parameter	T_1 (°C)	m_{wf} (kg·s ⁻¹)	T_4 (°C)	T_5 (°C)	W_{net} (kW)	Q_h (kW)	η_{ORC} (%)
Kaşka, Ö [55]	92.9	11.06	34.9	35.4	262.2	2479	10.58
Present study	93.3	11.06	34.87	35.41	244.6	2313	10.57
Error (%)	0.43	0	0.09	0.03	6.71	6.69	0.09

4. Results and Discussions

4.1. Dynamic Output Characteristics

Figure 5 shows a range of daily solar collector outlet temperatures which are adopted from the reference [52]. The climatic data is made up of annually average temperatures for each hour of the day. Solar hot water with different temperatures ranging from 34 °C to 122.6 °C is adopted to drive the ORC system, and the evaporating temperature is fixed at 80 °C. Figure 6 indicates the cumulative power output of the conventional solar ORC based on daily solar collector outlet temperatures in Figure 5. Results demonstrate that the cumulative power output of the solar ORC has the same trend in terms of three working fluids. The power generation process starts only if the outlet temperature of solar collector exceeds the evaporating temperature. The cumulative power output from the ORC increases considerably while the collector outlet temperature is higher than 80 °C. It can be noted that the ORC using isobutane shows a better performance than those using R245fa and R134a, and it has the highest cumulative work of 52 MJ. The maximum cumulative work can reach 31 MJ and 26 MJ by using R245fa and R134a, respectively.

Figure 7 shows a comparison of power output using three working fluids under a range of collector outlet temperatures. It can be observed that the net power output increases with the increase of outlet temperature. This is mainly because when the solar hot water outlet temperature increases, the expander inlet temperature will accordingly increase, which leads to a higher power output. The optimum outlet temperature is found to be 122.6 °C of which the maximum net power output can be obtained. It is indicated that the fluid isobutane still performs well when compared with the other working fluids, and it has the highest power output of 149 W. For working fluids R245fa and R134a, the maximum power outputs could reach 87 W and 77 W, respectively.

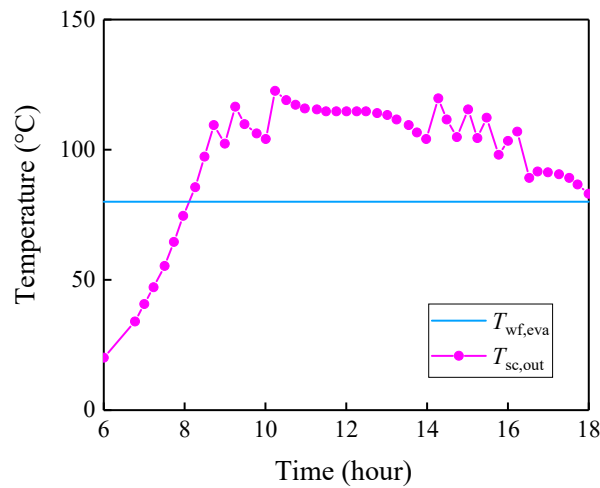


Figure 5. Daily solar collector outlet temperature vs. time [52].

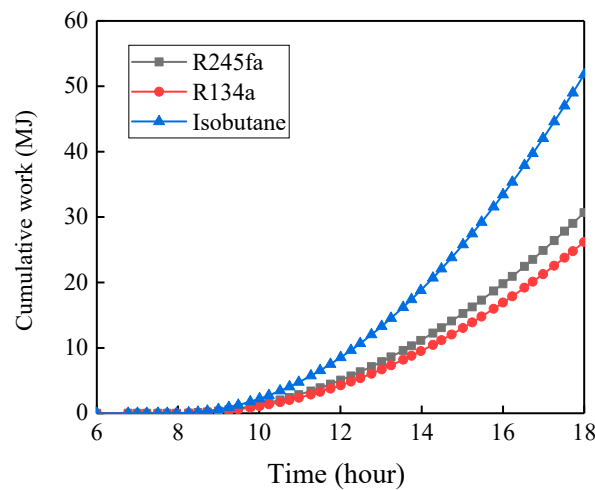


Figure 6. Cumulative power output based on daily solar collector outlet temperatures.

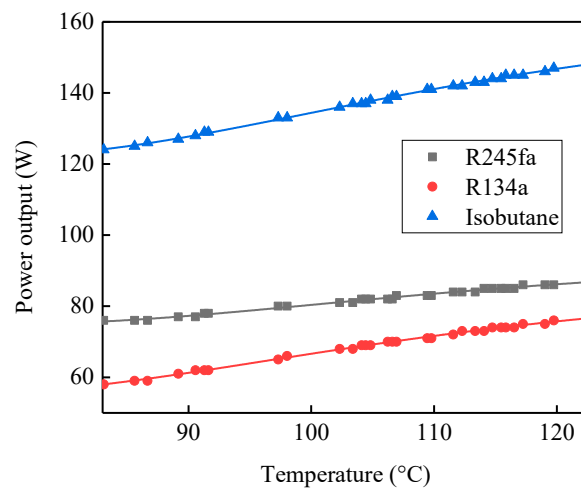


Figure 7. Net power output as a function of the solar collector outlet temperature.

4.2. Parametric Analysis

In this section, a parametric analysis was undertaken to compare the performance between solar ORCs using and not using TDP. Following variables are considered for power outputs of the systems: (1) evaporating temperature, T_{evap} ; (2) condensation temperature, T_{cond} ; (3) ORC working

fluid flow rate, \dot{m}_{wf} ; (4) fluid flow rate of solar collector, \dot{m}_{sc} ; (5) isentropic efficiency of the expander; (6) efficiency of heat exchanger. A single parameter was adjusted while the others were held constant in the parametric analysis. The solar collector outlet temperature is selected for the optimum power output in the simulation, i.e., 122.6 °C. Considering the solar ORC using TDP, the periods for the pre-expansion process and power generation under the condition of different parameters were selected based on the results of our previous experimental work [50]. R134 is selected as a typical working fluid which aims to show the minimum influence by using TDP.

Figure 8 reveals the power outputs of the solar ORC using and not using TDP when the evaporating temperature varies from 75 °C to 100 °C. It is worth noting that the power output of the solar ORC using TDP ranges from 72 W to 82 W, which is improved by up to 3.3% at a 100 °C evaporating temperature when compared with that of the conventional ORC. It is demonstrated that the power output for conventional ORC system climbs slightly from 90 °C to 95 °C and then fall rapidly after 95 °C. This is mainly due to the fact that with an increase of the evaporating temperature, the working fluid requires more heat for evaporation, which results in a decrease in the superheating capacity of the working fluid when constant heat is transferred by the solar collector. Then, the decrease in the expander inlet pressure leads to the decline in power output. Additionally, the power output of the solar ORC with TDP is higher than that of the conventional ORC when the evaporating temperature is higher than 90 °C. This is mainly because the working fluid pump consumes more electricity when the evaporating temperature increases, which exceeds the difference between the power output of the ORC using TDP and that of the conventional ORC. Thus, increased power output is achieved using the ORC with TDP in comparison with that using the conventional ORC.

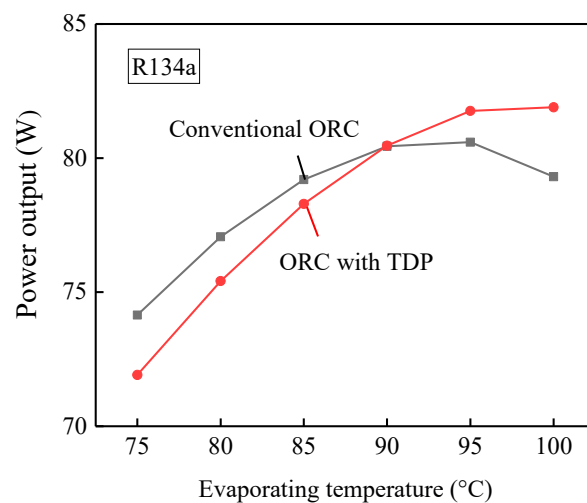


Figure 8. Power outputs of two solar ORCs vs. different evaporating temperatures.

Figure 9 indicates that the power outputs of both solar ORCs when the working fluid condensation temperature is increased from 15 °C to 35 °C. With the increasing of condensation temperature, the expander outlet pressure increases, thus the decreases of 30.5% are found in power outputs for the ORC with TDP and 33.6% for the conventional ORC. The working fluid can be fully cooled down to saturated liquid for more power output when the temperature of cooling water is lower. The power outputs of solar ORCs using and not using TDP range from 61.8 W to 88.9 W and 58.8 W to 88.5 W, respectively. The difference between two ORCs becomes larger with the increment of condensation temperature since conventional ORC generates less work at higher condensation temperature.

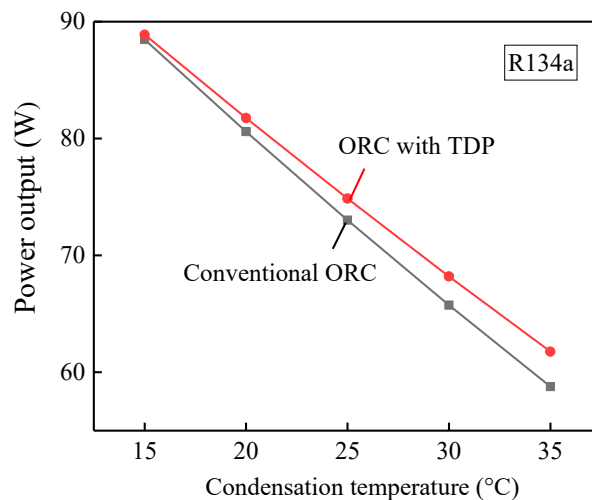


Figure 9. Power outputs of two solar ORCs vs. different condensation temperatures.

Figure 10 illustrates the power outputs of two ORCs with the increase in solar collector fluid mass flow rate. Given that the flow rate of solar collector fluid varies from $0.01 \text{ kg}\cdot\text{s}^{-1}$ to $0.2 \text{ kg}\cdot\text{s}^{-1}$, the work outputs of ORCs using and not using TDP tend to be steady at solar collector mass flow rate above $0.05 \text{ kg}\cdot\text{s}^{-1}$. It can be noted that the rapid rise of power output exists before flow rate of $0.05 \text{ kg}\cdot\text{s}^{-1}$. This is mainly because lower solar fluid flow rate which has a higher outlet temperature will lead to more superheating capacity of the working fluid. The increase of the expander inlet pressure leads to considerable increment in power output. It is also observed that the power output of ORC with TDP approaches that of conventional ORC with the increase of solar collector fluid flow rate. Because flow rate of solar collector fluid has little influence on pump work, thus the difference of power output between two solar ORCs could be negligible when the collector fluid flow rate infinitely increases.

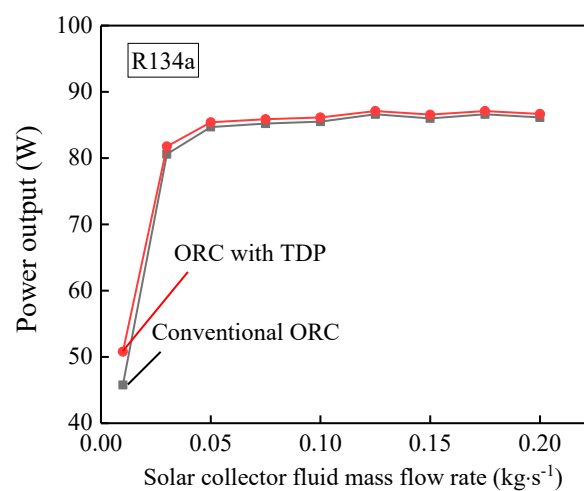


Figure 10. Power outputs of two solar ORCs vs. various mass flow rates of solar collector fluid.

The work outputs of two solar ORCs in terms of various ORC working fluid mass flow rates are also observed in Figure 11. Similar to Figure 10, the power output of conventional ORC tends to be flat when refrigerant flow rate varies from $0.001 \text{ kg}\cdot\text{s}^{-1}$ to $0.02 \text{ kg}\cdot\text{s}^{-1}$. The higher flow rate reduces the degree of superheating capacity required to operate the expander. In contrast, the power output of ORC with TDP keeps increasing with the increment of flow rate. Additionally, the difference of power output between two solar ORCs escalates as the working fluid mass flow rate increases. It is mainly because the larger flow rate results in higher pump work of conventional ORC, which enlarges their difference of power outputs.

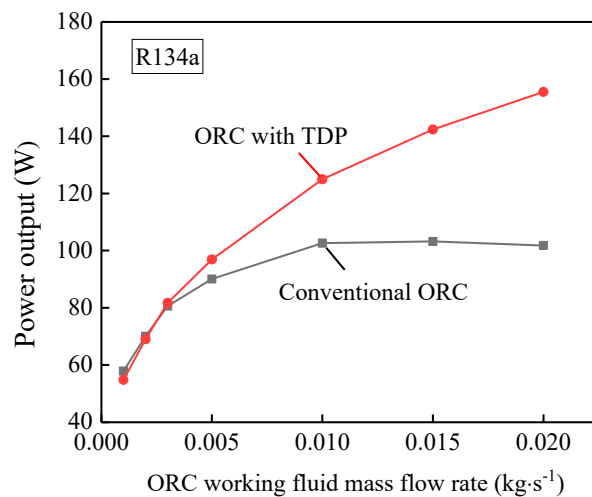


Figure 11. Power outputs of two solar ORCs vs. various working fluid mass flow rates.

In reality, the isentropic efficiencies of the working fluid pump and expander of small-scale ORC systems may be even lower than those of the simulation in this paper, i.e., 0.65 and 0.75, due to the limited selection and inappropriate design of ORC systems. Therefore, the relatively higher power output can be obtained from the ORC with TDP, which is quite competitive with the conventional ORC in household applications. With the decline of pump efficiency, the conventional ORC has a higher pump work which results in a lower power output. In contrast, the power output of ORC with TDP keeps constant at various pump efficiencies. It is also worth noting that the isentropic efficiency of the expander varies dramatically with regard to different external partial loads in real applications. Figure 12 shows the generated power outputs of two solar ORCs when the isentropic efficiency varies from 0 to 0.75. It is demonstrated that the ORC with TDP has a superior power output when compared with that of the conventional ORC. With the increment of isentropic efficiency, the difference of generated power of two solar ORCs decreases. The isentropic efficiency of expander selected in our previous experimental work ranges from 0.42 to 0.6 in terms of various partial loads [50]. Under this scenario, the power outputs of two solar ORCs range from 40 W to 62 W and from 46 W to 65 W, respectively. In ideal operation conditions, the isentropic efficiency of this expander can vary from 0.4 to 0.75. When the isentropic efficiency is 0.75, the maximum power output of two solar ORCs are 80.6 W and 81.8 W, respectively, which could indicate the minimum influence using TDP as mentioned above.

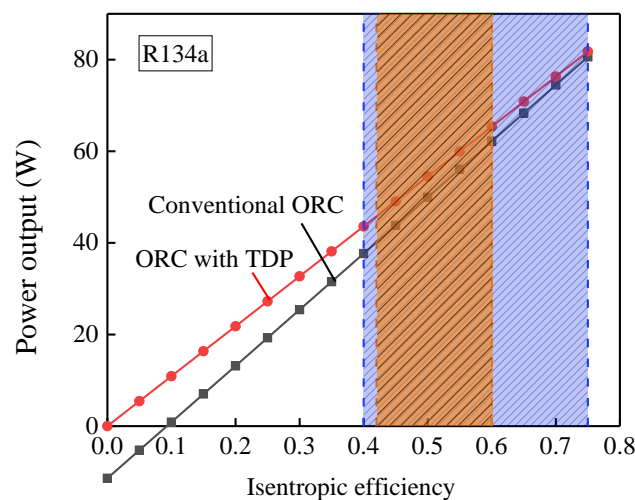


Figure 12. Power outputs of two solar ORCs vs. different isentropic efficiencies of expander.

Figure 13 also shows the results of power outputs when the heat exchangers efficiency varies. It can be observed that two solar ORCs have similar increasing trends with the increment of heat exchanger efficiency. ORC using TDP still performs better than conventional ORC. In the most cases, the heat exchanger efficiency is above 0.9. Thus, the power outputs of ORCs using and not using TDP at this interval range from 80.7 W to 81.8 W, and 79.4 W to 80.6 W, respectively.

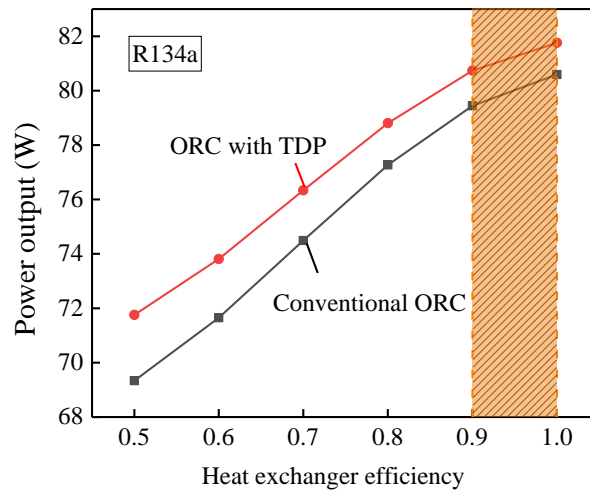


Figure 13. Power output of two solar ORCs vs. heat exchangers efficiencies.

4.3. Thermal Performance of Solar ORCs throughout the Day

This section aims to investigate the thermal performance of solar ORCs using and not using TDP in terms of various evaporating temperatures. Similar with Section 4.2, the solar collector outlet temperature is set as 122.6 °C for the maximum power output. Figure 14 indicates the energy and exergy efficiencies of the solar ORC using TDP when compared with those of the conventional ORC, with R134a as the working fluid. Figure 14a demonstrates that the energy efficiency of the solar ORC using TDP increases with the increase in evaporating temperature. When the temperature increases from 75 °C to 100 °C, the energy efficiency ranges from 11.3% to 12.6%. In order to further illustrate the significance of solar ORC using TDP, the energy efficiencies of two systems are compared with the results from references [1,10,56]. It is indicated that the energy efficiencies in the present work are much higher than the results from references [10,56] which are 8.58% and 5.6% when evaporating temperatures are 78.8 °C and 85 °C, respectively. It proves that the high efficiency evacuated flat-plate collector used in this study could supply a higher solar collector outlet temperature, which improves the overall energy efficiency of system. The difference of energy efficiency between present work and reference [1] is relatively small which is mainly because different working fluid flow rates. The efficiency of ORC using TDP is quite desirable when considering that the heat source temperature is relatively low, and it represents an advantage of the ORC using TDP. Similar to power output, the energy efficiency of the ORC using TDP becomes higher than that of conventional ORC when the temperature is higher than 90 °C. The difference in energy efficiency between the two solar ORCs increases remarkably with the increase in evaporating temperature. The largest percent increment in energy efficiency can reach 3.27% at a 100 °C evaporating temperature when compared with the conventional ORC. A similar trend for exergy efficiency can be found for the ORC using TDP, as shown in Figure 14b. Exergy efficiency ranges from 45.8% to 51.3% when the evaporating temperature increases from 75 °C to 100 °C. Results show that both energy efficiency and exergy efficiency of conventional ORC climb from 75 °C to 90 °C, followed by a slight increase, and it then decline rapidly from 95 °C to 100 °C. The main reason for the improved energy efficiency and exergy efficiency is that a higher power output is obtained from the ORC with TDP.

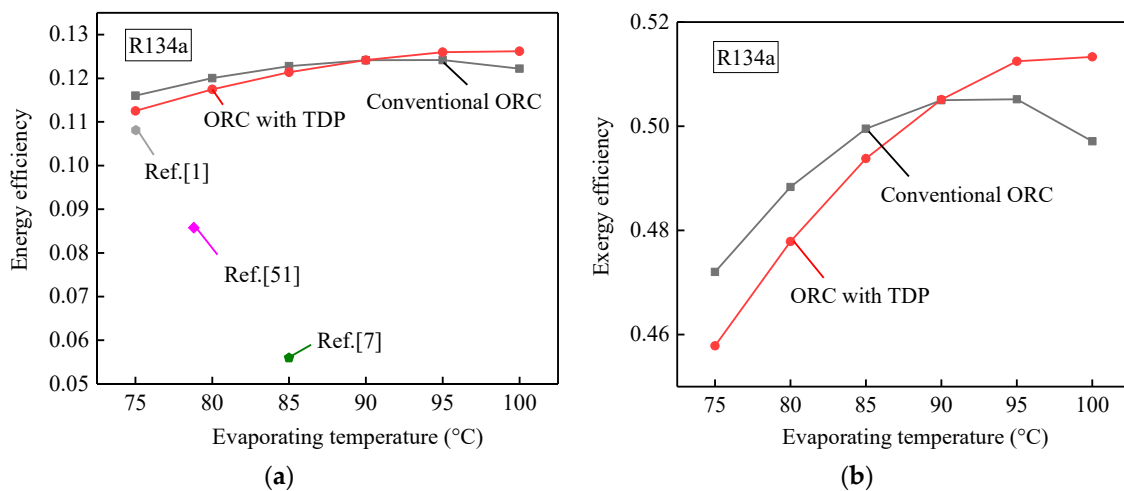


Figure 14. Energy and exergy efficiencies of two solar ORCs (a) energy efficiency; and (b) exergy efficiency.

Figure 15 shows the exergy destruction in each system component for solar ORCs using and not using TDP under the conditions of a 95 °C evaporating temperature and a 122.6 °C solar collector outlet temperature. Considering the conventional ORC system, it is worth noting that the majority of the exergy is lost in the preheater, expander, evaporator and condenser. This is inevitable when solar thermal is converted to mechanical work. The maximum amount of heat can be transferred in the preheater, which results in a largest difference between the output and inlet exergy of the preheater. It is indicated that the exergy destruction of the ORC using TDP can be reduced 2.86 W when eliminating the pump. Additionally, the exergy destruction is reduced in the evaporator and condenser by up to 92% and 2%, respectively. In contrast, the exergy destruction increases in the expander, preheater, superheater and regenerator. The increased exergy destruction in the heat exchangers is probably due to the larger temperature difference between the entering and exiting fluids of the component. Another reason is that the preheater has a lower inlet temperature, and the regenerator and superheater could have lower outlet temperatures of the working fluid during the pre-expansion process of the ORC using TDP. Since no power is generated from the expander during the pre-expansion process, it brings about a higher exergy destruction in the expander when compared with that of the conventional ORC operating within the same cycle time.

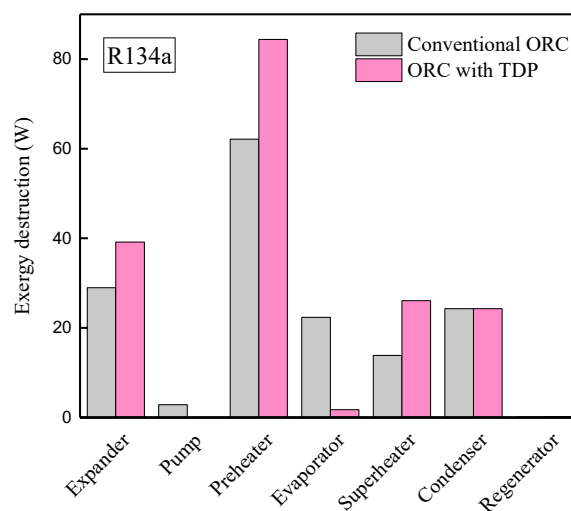


Figure 15. Exergy destruction of each component between two solar ORCs using R134a.

The exergy efficiency of each system component for both solar ORCs when using R134a is shown in Figure 16. It can be observed that the expander has the maximum exergy efficiency of 76% for the conventional ORC. The fluid pump also has a relatively higher exergy efficiency of 74.9%. An improved exergy efficiency of the evaporator can be observed for the solar ORC using TDP. The highest exergy efficiency of the evaporator can reach 96.9% for the ORC, and this is improved by 62% when compared with that of the conventional ORC, i.e., 59.9%. In contrast, the other components show relatively lower exergy efficiencies, especially for the preheater, which has the lowest exergy efficiency of 21.5%. This is mainly because the temperature of the working fluid increases gradually during the pre-expansion process, which may result in a lower inlet temperature of the working fluid.

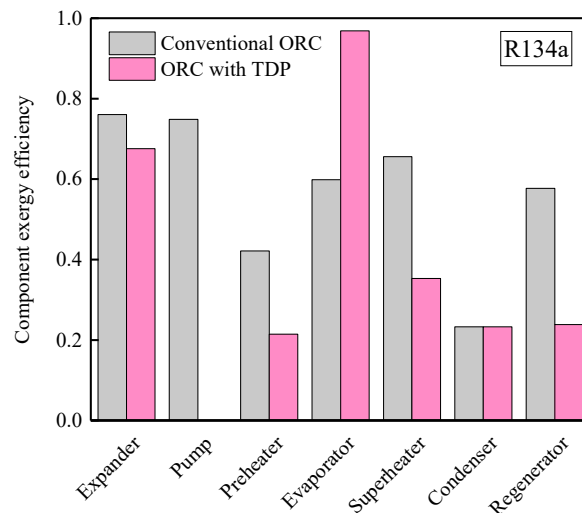


Figure 16. Exergy efficiency of each component between two solar ORCs using R134a.

4.4. Further Exploration and Comparison

In order to have a comprehensive understanding for small-scale household application, the solar ORC using TDP is compared with the conventional solar ORC in terms of system type, system compactness, power output stability, thermal efficiency and capital cost, as shown in Table 6. The conventional ORC is a continuous system, whereas the ORC using TDP is an intermittent system. The system compactness of the solar ORC with TDP is superior to that of the conventional ORC due to the elimination of the fluid pump. In many small-scale ORC experimental rigs, the fluid pump accounts for 5–10% of the system volume, which can then be reduced by using the ORC with TDP. Considering power output stability, the conventional ORC has a better performance than the solar ORC with TDP. It is worth noting that the relatively large fluctuation of the ORC with TDP may happen when the condenser and evaporator are mutually altered. However, this only lasts for a very short period, i.e., less than 10% of the cycle time when considering the total working process. For the solar energy utilisation of a household, efficient battery technology is expected to solve this problem. This means that the electricity is stored and then output constantly. Another possible solution is the introduction of more heat exchangers to the ORC with TDP, with the aim of ensuring that the evaporator is always generating power while other heat exchangers are either used for supplementing the working fluid or for condensation. However, this method may have a small influence on the system compactness, which could be the focus of our future work. Based on the above thermal analysis, the energy and exergy efficiencies of the solar ORC with TDP are higher than those of the conventional ORC in most operation cases. This improvement will become more advantageous to household application when the heat source temperature and scale of the system decrease. As for cost, the main difference between the ORC with TDP and the conventional ORC lies in the working fluid pump. The cost of the working fluid pump is usually 2–3 times higher than that of the heat exchanger in small-scale ORC applications. Thus, the total cost of the ORC using TDP could be reduced by at least 10% with regard to that of the

whole system. In general, the solar ORC using TDP is superior to the conventional ORC, which reveals the vast potential for small-scale household application, especially for places that have relatively low solar radiation.

Table 6. Comparison between the conventional ORC and ORC with TDP driven by solar energy.

Type	System Type	System Compactness	Output Stability	Energy Efficiency	Cost
Conventional ORC	Continuous	Moderate	High	Low	High
ORC using TDP	Intermittent	High	Low	Moderate	At least 10% less

5. Conclusions

In this paper, small-scale ORC systems driven by solar energy are presented to investigate the overall performance in terms of the power output, energy efficiency, exergy efficiency and exergy destruction of the components. Additionally, the thermal performance of the ORC using TDP is compared with that of the conventional ORC. The parametric analysis of two solar ORCs demonstrates that ORC with TDP has a superior performance to that of the conventional ORC under most working conditions. The power output of the solar ORC using TDP ranges from 72 W to 82 W when R134a is adopted as the working fluid and the evaporating temperature varies from 75 °C to 100 °C. The performance is improved by up to 9.5% at a 100 °C evaporating temperature when compared with that of the conventional ORC. The energy and exergy efficiencies of the ORC using TDP increase from 11.3% to 12.6% and from 45.8% to 51.3% when the evaporating temperature increases from 75 °C to 100 °C. For the ORC using TDP, the exergy destruction in the evaporator and condenser can be reduced by up to 92% and 2%, respectively. The highest exergy efficiency of the evaporator is 96.9% by using R134a, and this is an improvement of 62% compared with 59.9% of the conventional ORC. For small-scale solar utilisation, the ORC using TDP is almost superior to the conventional ORC in terms of system type, system compactness, power output stability, thermal efficiency and capital cost. The large fluctuation of the ORC using TDP may last a very short period during the switch of heat exchangers, which could be solved by using efficient battery technology. This technology could be an alternative to household power supply and also serves as the main part of solar heating and power generation.

Author Contributions: Conceptualization: R.W. and L.J.; methodology: R.W. and A.G.D.; supervision: L.J., Y.W., and A.P.R.; project administration: L.J., Z.M., and A.P.R.

Funding: This research was funded by the National Natural Science Foundation of China under grant number 51606118 and Heat-STRESS project EP/N02155X/1.

Acknowledgments: This research was supported by National Natural Science Foundation of China under contract number 51606118 and Heat-STRESS project EP/N02155X/1 funded by Engineering and Physical Science Research Council of UK.

Conflicts of Interest: The authors declare no conflict of interest.

Nomenclature

A	Area of solar collector, m^2
c	Specific heat capacity, $J \cdot kg^{-1}$
c_1	Collector heat loss coefficient, $W \cdot m^{-2} \cdot K^{-1}$
c_2	Temperature dependence of the heat loss coefficient, $W \cdot m^{-2} \cdot K^{-2}$
c_3	Wind speed dependence of the heat loss coefficient, $J \cdot m^{-3} \cdot K^{-1}$
c_4	Long-wave irradiance dependence of the heat loss coefficient
c_5	Solar collector effective thermal capacity, $J \cdot m^{-2} \cdot K^{-1}$
c_6	Wind-dependence of the collector optical (zero-loss) efficiency, $s \cdot m^{-1}$
E	Radiation (outside solar spectrum) onto the collector plane, $W \cdot m^{-2}$
\dot{E}	Exergy flow rate, W

e	Specific flow exergy, $W \cdot kg^{-1}$
F'	Collector efficiency factor
h	Specific enthalpy, $J \cdot kg^{-1}$
I	Irradiance, $W \cdot m^{-2}$
\dot{I}	Irreversibility rate, W
K_0	Solar collector Incident Angle Modifier
M	Mass, kg
\dot{m}	Mass flow rate, $kg \cdot s^{-1}$
\dot{Q}	Heat flow rate, W
s	Specific entropy, $J \cdot kg^{-1} \cdot K^{-1}$
t	Time, s
T	Temperature, K
u	Wind speed in (parallel to) the collector plane, $m \cdot s^{-1}$
V	Valve
W	Work, W

Greek Letters

η	Efficiency
θ	Incidence angle, $^\circ$
ρ	Density, $kg \cdot m^{-3}$
$(\tau\alpha)$	Effective transmittance-absorptance product

Subscripts

0	Dead state
ave	Average
b	Direct (beam) radiation
c	Cooling water
d	Diffuse radiation
cond	Condenser
eva	Evaporator
ex	Exergy
exp	Expander
ext	External environment
h	Heat
in	Inlet
ins	Instantaneous power output
L	Long wavelength
net	Net power output
out	Outlet
p	Isobaric process
pu	Pump
preheat	Preheater
regen	Regenerator
s	Isentropic
sc	Solar collector
sol	Solar
superheat	Superheater
superheated	Superheated temperature
v	Vapor
w	Water
wf	Working fluid

Abbreviations

ORC	Organic Rankine cycle
RV	Refrigerant valve
TDP	Thermal driven pump

References

1. Freeman, J.; Hellgardt, K.; Markides, C.N. Working fluid selection and electrical performance optimisation of a domestic solar-ORC combined heat and power system for year-round operation in the UK. *Appl. Energy* **2017**, *186*, 291–303. [[CrossRef](#)]
2. Chen, Z.-G.; Shi, X.; Zhao, L.-D.; Zou, J. High-performance SnSe thermoelectric materials: Progress and future challenge. *Prog. Mater. Sci.* **2018**, *97*, 283–346. [[CrossRef](#)]
3. Yang, L.; Chen, Z.-G.; Dargusch, M.S.; Zou, J. High Performance Thermoelectric Materials: Progress and Their Applications. *Adv. Energy Mater.* **2018**, *8*, 1701797. [[CrossRef](#)]
4. Cioccolanti, L.; Tascioni, R.; Arteconi, A. Mathematical modelling of operation modes and performance evaluation of an innovative small-scale concentrated solar organic Rankine cycle plant. *Appl. Energy* **2018**, *221*, 464–476. [[CrossRef](#)]
5. Freeman, J.; Hellgardt, K.; Markides, C.N. An assessment of solar-powered organic Rankine cycle systems for combined heating and power in UK domestic applications. *Appl. Energy* **2015**, *138*, 605–620. [[CrossRef](#)]
6. Freeman, J.; Hellgardt, K.; Markides, C.N. An Assessment of Solar-Thermal Collector Designs for Small-Scale Combined Heating and Power Applications in the United Kingdom. *Heat Transf. Eng.* **2015**, *36*, 1332–1347. [[CrossRef](#)]
7. Tzivanidis, C.; Bellos, E.; Antonopoulos, K.A. Energetic and financial investigation of a stand-alone solar-thermal Organic Rankine Cycle power plant. *Energy Convers. Manag.* **2016**, *126*, 421–433. [[CrossRef](#)]
8. Petrollese, M.; Cocco, D. Robust optimization for the preliminary design of solar organic Rankine cycle (ORC) systems. *Energy Convers. Manag.* **2019**, *184*, 338–349. [[CrossRef](#)]
9. Casartelli, D.; Binotti, M.; Silva, P.; Macchi, E.; Roccaro, E.; Passera, T. Power Block Off-design Control Strategies for Indirect Solar ORC Cycles. *Energy Procedia* **2015**, *69*, 1220–1230. [[CrossRef](#)]
10. Quoilin, S.; Orosz, M.; Hemond, H.; Lemort, V. Performance and design optimization of a low-cost solar organic Rankine cycle for remote power generation. *Sol. Energy* **2011**, *85*, 955–966. [[CrossRef](#)]
11. Canada, S.; Cohen, G.; Cable, R.; Brosseau, D.; Price, H. *Parabolic Trough Organic Rankine Cycle Power Plant*; No. NREL/CP-550-37077; National Renewable Energy Lab (NREL): Golden, CO, USA, 2005.
12. Bellos, E.; Tzivanidis, C. Parametric analysis and optimization of an Organic Rankine Cycle with nanofluid based solar parabolic trough collectors. *Renew. Energy* **2017**, *114*, 1376–1393. [[CrossRef](#)]
13. Manolakos, D.; Kosmadakis, G.; Kyritsis, S.; Papadakis, G. On site experimental evaluation of a low-temperature solar organic Rankine cycle system for RO desalination. *Sol. Energy* **2009**, *83*, 646–656. [[CrossRef](#)]
14. Freeman, J.; Guarracino, I.; Kalogirou, S.A.; Markides, C.N. A small-scale solar organic Rankine cycle combined heat and power system with integrated thermal energy storage. *Appl. Therm. Eng.* **2017**, *127*, 1543–1554. [[CrossRef](#)]
15. Manfrida, G.; Secchi, R.; Stańczyk, K. Modelling and simulation of phase change material latent heat storages applied to a solar-powered Organic Rankine Cycle. *Appl. Energy* **2016**, *179*, 378–388. [[CrossRef](#)]
16. Jing, L.; Gang, P.; Jie, J. Optimization of low temperature solar thermal electric generation with Organic Rankine Cycle in different areas. *Appl. Energy* **2010**, *87*, 3355–3365. [[CrossRef](#)]
17. Shi, L.; Shu, G.; Tian, H.; Deng, S. A review of modified Organic Rankine cycles (ORCs) for internal combustion engine waste heat recovery (ICE-WHR). *Renew. Sustain. Energy Rev.* **2018**, *92*, 95–110. [[CrossRef](#)]
18. Braimakis, K.; Karellas, S. Energetic optimization of regenerative Organic Rankine Cycle (ORC) configurations. *Energy Convers. Manag.* **2018**, *159*, 353–370. [[CrossRef](#)]
19. Wang, X.D.; Zhao, L.; Wang, J.L. Experimental investigation on the low-temperature solar Rankine cycle system using R245fa. *Energy Convers. Manag.* **2011**, *52*, 946–952. [[CrossRef](#)]
20. Chen, H.; Goswami, D.Y.; Stefanakos, E.K. A review of thermodynamic cycles and working fluids for the conversion of low-grade heat. *Renew. Sustain. Energy Rev.* **2010**, *14*, 3059–3067. [[CrossRef](#)]
21. Bao, J.; Zhao, L. A review of working fluid and expander selections for organic Rankine cycle. *Renew. Sustain. Energy Rev.* **2013**, *24*, 325–342. [[CrossRef](#)]
22. Shu, G.; Zhao, J.; Tian, H.; Liang, X.; Wei, H. Parametric and exergetic analysis of waste heat recovery system based on thermoelectric generator and organic rankine cycle utilizing R123. *Energy* **2012**, *45*, 806–816. [[CrossRef](#)]

23. Wei, D.; Lu, X.; Lu, Z.; Gu, J. Dynamic modeling and simulation of an Organic Rankine Cycle (ORC) system for waste heat recovery. *Appl. Therm. Eng.* **2008**, *28*, 1216–1224. [[CrossRef](#)]
24. Mago, P.J.; Chamra, L.M.; Srinivasan, K.; Somayaji, C. An examination of regenerative organic Rankine cycles using dry fluids. *Appl. Therm. Eng.* **2008**, *28*, 998–1007. [[CrossRef](#)]
25. Nguyen, V.M.; Doherty, P.S.; Riffat, S.B. Development of a prototype low-temperature Rankine cycle electricity generation system. *Appl. Therm. Eng.* **2001**, *21*, 169–181. [[CrossRef](#)]
26. Wang, X.D.; Zhao, L. Analysis of zeotropic mixtures used in low-temperature solar Rankine cycles for power generation. *Sol. Energy* **2009**, *83*, 605–613. [[CrossRef](#)]
27. Wang, J.L.; Zhao, L.; Wang, X.D. A comparative study of pure and zeotropic mixtures in low-temperature solar Rankine cycle. *Appl. Energy* **2010**, *87*, 3366–3373. [[CrossRef](#)]
28. Shu, G.; Wang, X.; Tian, H.; Liu, P.; Jing, D.; Li, X. Scan of working fluids based on dynamic response characters for Organic Rankine Cycle using for engine waste heat recovery. *Energy* **2017**, *133*, 609–620. [[CrossRef](#)]
29. Yang, J.; Sun, Z.; Yu, B.; Chen, J. Experimental comparison and optimization guidance of R1233zd(E) as a drop-in replacement to R245fa for organic Rankine cycle application. *Appl. Therm. Eng.* **2018**, *141*, 10–19. [[CrossRef](#)]
30. Ayachi, F.; Ksayer, E.B.; Neveu, P.; Zoughaib, A. Experimental investigation and modeling of a hermetic scroll expander. *Appl. Energy* **2016**, *181*, 256–267. [[CrossRef](#)]
31. Jiang, L.; Lu, H.; Wang, R.; Wang, L.; Gong, L.; Lu, Y.; Roskilly, A.P. Investigation on an innovative cascading cycle for power and refrigeration cogeneration. *Energy Convers. Manag.* **2017**, *145*, 20–29. [[CrossRef](#)]
32. Garg, P.; Karthik, G.M.; Kumar, P.; Kumar, P. Development of a generic tool to design scroll expanders for ORC applications. *Appl. Therm. Eng.* **2016**, *109 Pt B*, 878–888. [[CrossRef](#)]
33. Gao, P.; Jiang, L.; Wang, L.W.; Wang, R.Z.; Song, F.P. Simulation and experiments on an ORC system with different scroll expanders based on energy and exergy analysis. *Appl. Therm. Eng.* **2015**, *75*, 880–888. [[CrossRef](#)]
34. Hou, X.; Zhang, H.; Yu, F.; Liu, H.; Yang, F.; Xu, Y.; Tian, Y.; Li, G. Free piston expander-linear generator used for organic Rankine cycle waste heat recovery system. *Appl. Energy* **2017**, *208*, 1297–1307. [[CrossRef](#)]
35. Baccioli, A.; Antonelli, M.; Desideri, U. Dynamic modeling of a solar ORC with compound parabolic collectors: Annual production and comparison with steady-state simulation. *Energy Convers. Manag.* **2017**, *148*, 708–723. [[CrossRef](#)]
36. Papes, I.; Degroote, J.; Vierendeels, J. New insights in twin screw expander performance for small scale ORC systems from 3D CFD analysis. *Appl. Therm. Eng.* **2015**, *91*, 535–546. [[CrossRef](#)]
37. Ziviani, D.; Suman, A.; Lecompte, S.; De Paepe, M.; van den Broek, M.; Spina, P.R.; Pinelli, M.; Venturini, M.; Beyene, A. Comparison of a Single-screw and a Scroll Expander under Part-load Conditions for Low-grade Heat Recovery ORC Systems. *Energy Procedia* **2014**, *61*, 117–120. [[CrossRef](#)]
38. Kang, S.H. Design and experimental study of ORC (organic Rankine cycle) and radial turbine using R245fa working fluid. *Energy* **2012**, *41*, 514–524. [[CrossRef](#)]
39. Song, P.; Wei, M.; Liu, Z.; Zhao, B. Effects of suction port arrangements on a scroll expander for a small scale ORC system based on CFD approach. *Appl. Energy* **2015**, *150*, 274–285. [[CrossRef](#)]
40. Hou, X.; Zhang, H.; Xu, Y.; Yu, F.; Zhao, T.; Tian, Y.; Yang, Y.; Zhao, R. External load resistance effect on the free piston expander-linear generator for organic Rankine cycle waste heat recovery system. *Appl. Energy* **2018**, *212*, 1252–1261. [[CrossRef](#)]
41. Jiménez-Arreola, M.; Pili, R.; Wieland, C.; Romagnoli, A. Analysis and comparison of dynamic behavior of heat exchangers for direct evaporation in ORC waste heat recovery applications from fluctuating sources. *Appl. Energy* **2018**, *216*, 724–740. [[CrossRef](#)]
42. Dong, J.; Zhang, X.; Wang, J. Experimental investigation on heat transfer characteristics of plate heat exchanger applied in organic Rankine cycle (ORC). *Appl. Therm. Eng.* **2017**, *112*, 1137–1152. [[CrossRef](#)]
43. Borsukiewicz-Gozdur, A. Pumping work in the organic Rankine cycle. *Appl. Therm. Eng.* **2013**, *51*, 781–786. [[CrossRef](#)]
44. Tahir, M.B.I.N.M.; Yamada, N. Characteristics of Small ORC System for Low Temperature Waste Heat Recovery. *J. Environ. Eng.* **2009**, *4*, 375–385. [[CrossRef](#)]

45. Kim, D.K.; Lee, J.S.; Kim, J.; Kim, M.S.; Kim, M.S. Parametric study and performance evaluation of an organic Rankine cycle (ORC) system using low-grade heat at temperatures below 80 °C. *Appl. Energy* **2017**, *189*, 55–65. [[CrossRef](#)]
46. Yamada, N.; Minami, T.; Anuar Mohamad, M.N. Fundamental experiment of pumpless Rankine-type cycle for low-temperature heat recovery. *Energy* **2011**, *36*, 1010–1017. [[CrossRef](#)]
47. Akbarzadeh, A.; Johnson, P.; Nguyen, T.; Mochizuki, M.; Mashiko, M.; Sauciuc, I.; Kusaba, S.; Suzuki, H. Formulation and analysis of the heat pipe turbine for production of power from renewable sources. *Appl. Therm. Eng.* **2001**, *21*, 1551–1563. [[CrossRef](#)]
48. Yamada, N.; Watanabe, M.; Hoshi, A. Experiment on pumpless Rankine-type cycle with scroll expander. *Energy* **2013**, *49*, 137–145. [[CrossRef](#)]
49. Gao, P.; Wang, L.W.; Wang, R.Z.; Jiang, L.; Zhou, Z.S. Experimental investigation on a small pumpless ORC (organic rankine cycle) system driven by the low temperature heat source. *Energy* **2015**, *91*, 324–333. [[CrossRef](#)]
50. Jiang, L.; Lu, H.T.; Wang, L.W.; Gao, P.; Zhu, F.Q.; Wang, R.Z.; Roskilly, A.P. Investigation on a small-scale pumpless Organic Rankine Cycle (ORC) system driven by the low temperature heat source. *Appl. Energy* **2017**, *195*, 478–486. [[CrossRef](#)]
51. *Aspen Plus*, version 8.8; Aspen Technology, Inc.: Cambridge, UK, 2018; Available online: <https://www.aspentech.com/> (accessed on 7 November 2018).
52. Freeman, J.; Hellgardt, K.; Markides, C.N. *Towards the Optimization of a Domestic-Scale Organic Rankine System for Combined Heating and Power Provision in the UK*; Department of Chemical Engineering; Imperial College: London, UK, 2013; p. 53.
53. Perers., B.; Bales, C. A Solar Collector Model for TRNSYS Simulation and System Testing. *Report of IEA SHC—Task 26: Solar Combisystems*; International Energy Agency, Solar Heating & Cooling Programme, 2002. Available online: <https://www.aee-intec.at/0uploads/dateien55.pdf> (accessed on 7 November 2018).
54. BS EN 12975-2: Thermal solar systems and components. Solar collectors. *Test Methods* **2006**.
55. Kaşka, Ö. Energy and exergy analysis of an organic Rankine for power generation from waste heat recovery in steel industry. *Energy Convers. Manag.* **2014**, *77*, 108–117. [[CrossRef](#)]
56. Bekiloğlu, H.E.; Bedir, H.; Anlaş, G. Multi-objective optimization of ORC parameters and selection of working fluid using preliminary radial inflow turbine design. *Energy Convers. Manag.* **2019**, *183*, 833–847. [[CrossRef](#)]



© 2019 by the authors. Licensee MDPI, Basel, Switzerland. This article is an open access article distributed under the terms and conditions of the Creative Commons Attribution (CC BY) license (<http://creativecommons.org/licenses/by/4.0/>).